Frequency-Domain Modeling and Simulation of DC Power Electronic Systems Using Harmonic State Space Method

JunBum Kwon, *Student Member, IEEE*, Xiongfei Wang, *Member, IEEE*, Frede Blaabjerg, *Fellow, IEEE*, and Claus Leth Bak, *Senior Member, IEEE*

***Abstract*—For the efficiency and simplicity of electric systems, the dc power electronic systems are widely used in a variety of applications such as electric vehicles, ships, and aircraft and in homes. In these systems, there could be a number of dynamic interactions and frequency coupling between network and loads and other converters. Hence, time-domain simulations are usually required to consider such a complex system behavior. However, simulations in the time domain may increase the calculation time and the utilization of computer memory. Furthermore, frequency coupling driven by multiple converters with different switching frequencies or harmonics from ac–dc converters makes that harmonics and frequency coupling are both problems of ac system and challenges of dc system. This paper presents the modeling and simulation methods of a large dc system by using the harmonic state space (HSS) modeling. Through this method, the required computation time and CPU memory can be reduced, where this faster simulation can be an advantage of a large network simulation. Besides, the achieved results show the same results as that of the nonlinear time-domain simulation. Furthermore, the HSS modeling can describe how the frequency components are coupled with each other through the different switching frequency of each converter.**

***Index Terms*—DC distribution network, harmonic instability, harmonic state space (HSS) modeling.**

I. Introduction

DUE to the advantages such as high energy efficiency, lower line losses, and simple structure, the dc power electronic systems are becoming more used in a variety of application. For instance, electric ship, aircraft, home network, medical systems, and dc microgrid are important applications [1]–[4]. In these dc power electronic systems, the frequency coupling can happen due to the multiple connections of other converters, loads such as constant power loads, and control interaction [5]. These behaviors may cause the unexpected instability of the system as well as unknown steady-state harmonics in the output. As a result, it will bring EMI problem due to the high-frequency coupling [6], [7] and lower the efficiency of conversion process because of low-frequency coupling [8] as well. The harmonics and frequency coupling in the dc systems are new challenges to be analyzed with ac distribution systems because the dc is originally from ac–dc converters in the dc distribution network, meaning dc also contains the low-order harmonics, for instance, 100 and 200 Hz. Hence, a proper tool is required to analyze these interaction behaviors in the modeling and to emulate in the simulation.

Even though nonlinear time simulation can be considered as a solution, there are many difficulties in the case of large complex systems. The transient and steady-state simulations using switching models require a large computation memory and long-term simulation time due to a time-step variation for convergence. To overcome these difficulties, the several linearized models have been researched to analyze the complex behaviors.

The linearization of dc–dc converters has always been an important topic in the past few decades. The state-space averaging (SSAV) method was first developed for the linearization of dc–dc converters [5] to get rid of the time-discontinuous switching behavior of dc–dc converters. This modeling procedure has been commonly used for stability analysis and controller design of dc–dc converters. It is, however, assumed that the switching ripples are comparably small enough to be neglected and that the ratio of switching to fundamental frequency is high (i.e., high pulse ratio) such that the switching harmonics have no influence on the dynamics of the control system. This assumption may yield an inaccurate model with overlooking the dynamic frequency interactions of low pulse-ratio converters. In [9], the averaging model, which takes the influence of the time-varying effect of modulation into account, shows a better result than the original state-space averaging model. Hence, it is important to linearize the time-varying behavior of the model to analyze both dynamic control interactions and frequency coupling characteristics accurately.

To overcome the aforementioned limitations, several modeling methods were developed to include the time-varying effect in the converter models partially. First, the generalized averaging (also known as dynamic phasor) method (GAV) and multifrequency averaging technique were developed by including the influence of harmonics [10]–[12]. However, if multiharmonic components should be considered, the equation becomes nonlinear. The number of state variable vectors and the number of inputs can be different. Hence, the procedure for both linearization and simplification is necessarily required to

Manuscript received November 9, 2015; revised February 6, 2016; accepted March 14, 2016. Date of publication March 21, 2016; date of current version November 11, 2016. This paper was presented in part at the 2015 IEEE COMPEL (PELS-sponsored conference). This work was supported by the European Research Council (ERC) under the European Union's Seventh Framework Program (FP/2007–2013)/ERC Grant Agreement 321149-Harmony.

The authors are with the Department of Energy Technology, Aalborg University, 9220 Aalborg East, Denmark (e-mail: jbk@et.aau.dk; xwa@et.aau.dk; fbl@et.aau.dk; Clb@et.aau.dk).

Color versions of one or more of the figures in this paper are available online at http://ieeexplore.ieee.org.

Digital Object Identifier 10.1109/TPEL.2016.2544279

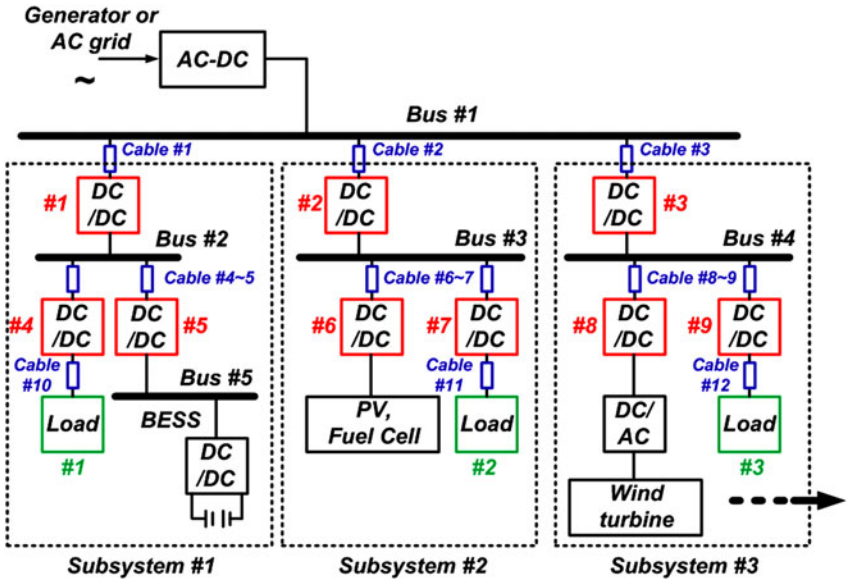

Fig. 1. Multiconverter dc power electronics system [nine dc–dc converters (#1 to #9), three dc loads (#1 to #3)]. BESS, battery energy storage system.

make it as a linearized model. The describing function is used to linearize the nonlinear equation in [10]. However, it means that the generalized averaging modeling method is also using the same assumption with the describing function. At the end of the procedure, it enforces the response as a single-input single-output (SISO) system and it cannot emulate the coupled response. Second, the ripple-theorem-based averaging models have been studied to model some specific topologies which cannot be modeled through the state-space averaging method [13], [14]. The single-input multiple-output (SIMO) topologies are modeled in [14] by using this theorem. The behaviors of an inductor ripple are divided into several stages according to the on and off status of switching, and each stage is averaged by including the ac components of switching. The obtained results show more accurate behavior than the traditional state-space averaging method. However, the basic background of this theory also starts from the averaging theory similar to the generalized averaging method. The averaged switching information may be difficult to represent the coupling behavior between input and output sides of dc–dc converters.

Third, the sampling-based model is also proposed in [15] and [16] to analyze the SIMO characteristic of the buck converter. The method describes how the perturbed input frequency can be transferred to the output frequency. The research found that the traditional modeling mainly focuses on the low-frequency perturbation and that the traditional way may be difficult to figure out the high-frequency behavior. However, the method is difficult to be used in the coupling analysis when the input voltage contains the multiple frequency information simultaneously.

Fourth, based on the theory of harmonic domain (HD) [17], extended harmonic domain (EHD) [18], and harmonic transfer function (HTF) [19], the harmonic state space (HSS) modeling methods are developed to linearize all time-varying components of the ac–dc converter, e.g., pulsewidth modulation, nonlinearities of passive components, and ac/dc disturbances [20]–[22] and to analyze the harmonic coupling and stability with additional harmonic impedances for complex systems, which cannot be found by the conventional approaches [23]. These methods have intuitively showed how frequencies are coupled to each other and how they interact with the controller dynamic and passive components. Furthermore, the basic structure of the HSS method is based on the multiple linear time-invariant (LTI) systems derived from the linear time-varying (LTV) periodic (LTP) system. Hence, the model has the feature of multiple-input multiple-output (MIMO) systems, and it makes the model to emulate the interaction between the multiple-frequency outputs and the multiple-frequency inputs.

This paper proposes a simulation model for dc power electronic systems using the HSS modeling method. First, the modeling procedures for dc–dc converters such as buck, boost, and buck–boost are explained briefly. Second, the multiparallel connected dc–dc converters are implemented based on the single dc–dc converter modeling results. Third, both the steady-state and dynamic characteristics of the converters are simulated by using the HSS method. Fourth, the frequency coupling characteristic is described with two case simulations. The analyzed results are verified by the time-domain and the frequency-domain simulations as well.

II. HSS Modeling Method for DC Power Electronic Systems

A. Review of HSS Modeling

The HSS modeling method is originally introduced to include time-varying elements in the linearized model. The LTV model is practically a nonlinear model because of the varying characteristic of the system parameters having a varying operating point. Hence, the model is difficult to be solved at a specific operating point such as in the linear time-invariant (LTI) model. However, if all signals are assumed to be varying periodically, it is possible to linearize the model by means of Fourier series. Based on these assumptions and definitions, the HSS model can have a format as shown in (1), where X_n is the harmonic

TABLE I
CIRCUIT DIAGRAM AND HSS MODELING OF DC–DC CONVERTERS FOR USE IN DC GRID: (A) BUCK CONVERTER, (B) BOOST CONVERTER, AND (C) BUCK–BOOST CONVERTER, WHERE *Z* IS THE ZERO MATRIX

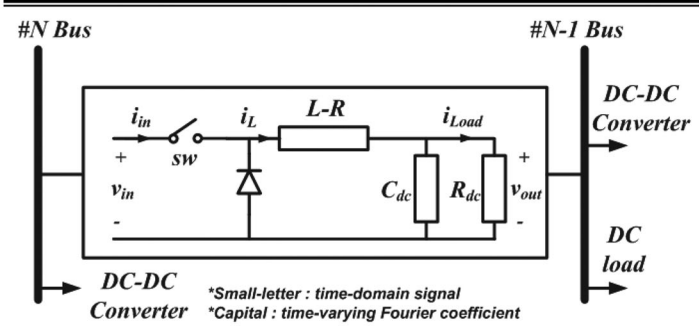 (a)	$$\begin{bmatrix} \dot{I}_L(t) \\ \dot{V}_{out}(t) \end{bmatrix} = \begin{bmatrix} -N & diag(-\frac{1}{L}) \\ diag(\frac{1}{C_{dc}}) & -N \end{bmatrix} \begin{bmatrix} I_L(t) \\ V_{out}(t) \end{bmatrix} + \begin{bmatrix} \frac{\Gamma(SW)}{L} & Z \\ Z & diag(-\frac{1}{C_{dc}}) \end{bmatrix} \begin{bmatrix} V_{in}(t) \\ I_{Load}(t) \end{bmatrix}$$ (4)
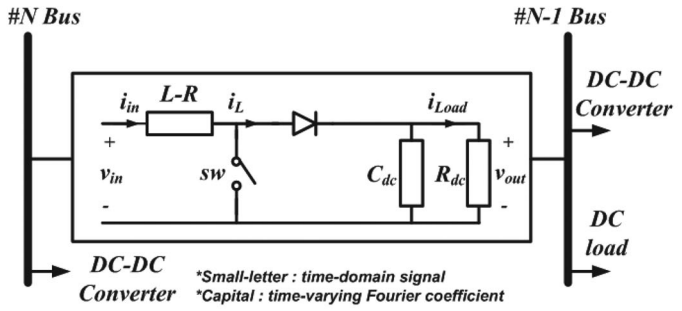 (b)	$$\begin{bmatrix} \dot{I}_L(t) \\ \dot{V}_{out}(t) \end{bmatrix} = \begin{bmatrix} -N & -\Gamma(1-SW) \\ \frac{\Gamma(1-SW)}{C_{dc}} & -N \end{bmatrix} \begin{bmatrix} I_L(t) \\ V_{out}(t) \end{bmatrix} + \begin{bmatrix} diag(\frac{1}{L}) & Z \\ Z & diag(-\frac{1}{C_{dc}}) \end{bmatrix} \begin{bmatrix} V_{in}(t) \\ I_{Load}(t) \end{bmatrix}$$ (5)
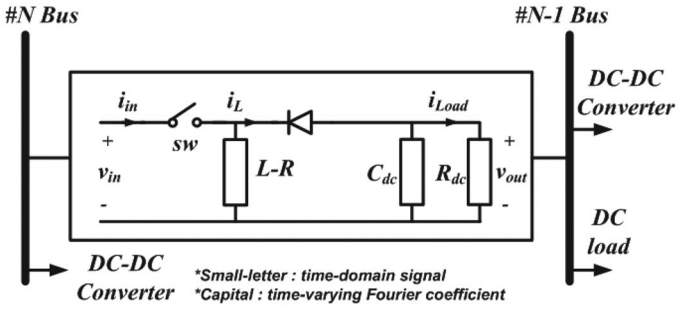 (c)	$$\begin{bmatrix} \dot{I}_L(t) \\ \dot{V}_{out}(t) \end{bmatrix} = \begin{bmatrix} -N & -\frac{\Gamma(1-SW)}{L} \\ \frac{\Gamma(1-SW)}{C_{dc}} & -N \end{bmatrix} \begin{bmatrix} I_L(t) \\ V_{out}(t) \end{bmatrix} + \begin{bmatrix} \frac{\Gamma(SW)}{L} & Z \\ Z & diag(-\frac{1}{C_{dc}}) \end{bmatrix} \begin{bmatrix} V_{in}(t) \\ I_{Load}(t) \end{bmatrix}$$ (6)

state matrix, Y_n is the output harmonic matrix, U_m is the input harmonic matrix, and A_{n-m} is the harmonic system matrix driven by the LTP theory [23]. B_{n-m}, C_{n-m}, and D_{n-m} are also the harmonic state matrices, which are dependent on the number of input and output. All the matrix sizes are dependent on the number of harmonics considered in the HSS modeling procedure

$$(s + jm\omega_0) X_n = \sum_{-\infty}^{\infty} A_{n-m} X_m + \sum_{-\infty}^{\infty} B_{n-m} U_m$$
$$Y_n = \sum_{-\infty}^{\infty} C_{n-m} X_m + \sum_{-\infty}^{\infty} D_{n-m} U_m. \quad (1)$$

Each time-varying harmonic vector (*X, U, Y*) can be transformed into the time domain by using

$$x(t) = P(t) X \quad (2)$$

where

$$P(t) = \left[e^{-jh\omega_0 t} \cdots e^{-j2\omega_0 t}, e^{-j\omega_0 t}, 1, e^{j\omega_0 t}, e^{j2\omega_0 t} \cdots e^{jh\omega_0 t}\right]$$
$$X = \left[X_{-h}(t) \cdots X_{-1}(t) X_0(t) X_1(t) \cdots X_h(t)\right]^T.$$

B. Topology Modeling

Based on the modeling procedure, all components can be modeled into the HSS formulation. A multiconverter dc power electronic system is shown in Fig. 1, where the dc–dc converters (#1 to #9) and dc loads (#1 to #3) are only considered in this paper. The other related converters such as a bidirectional dc–dc converter and an ac–dc converter are assumed as constant dc voltage/current sources. Based on (1), three principal converters (buck, boost, and buck–boost) are modeled according to the procedure described in [23] and [24]. Even though there are more various kinds of circuits and thus models such as full-bridge

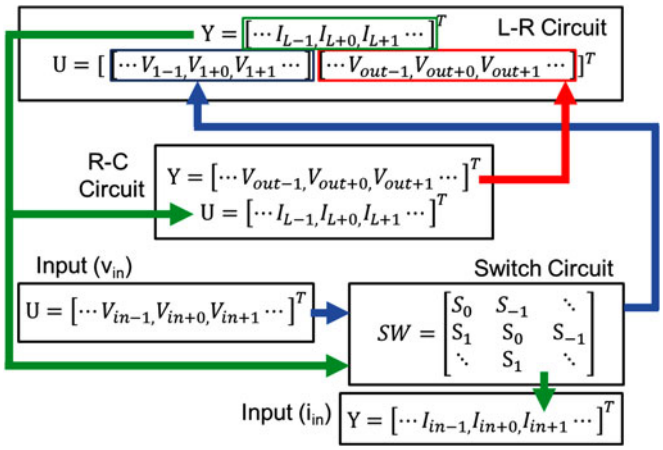

Fig. 2. Block diagram of the harmonics vector flow for calculation of buck converter.

type, interleaved converter, flyback converter, these topologies are also basically derived from three principal models.

According to (1) and (2), the topologies can be modeled as shown in Table I and (4)–(6), where "*N*" is derived from derivative of (1) as shown in (3), "diag(·)" means the diagonal matrix and "*Z*" means the zero matrix

$$N = \mathrm{diag}\left[-jk\omega_0 \ldots -j\omega_0,\ 0,\ j\omega_0, \ldots jk\omega_0\right] \tag{3}$$

In the case of a switching element, the harmonic components should be transformed into the Toeplitz matrix ($\Gamma(.)$) to perform a convolution. Furthermore, it is noted that the small variation term of switching vector ($\Gamma(\mathrm{SW})$) will be updated from the controller in every state change. Additionally, the number of harmonic vectors decides the accuracy of the modeling results. Hence, the optimized selection of both the fundamental frequency and the number of harmonics vector are an important criterion to do a fast and accurate simulation. In this paper, the fundamental frequency (f_o) is selected as 50 Hz to consider the low-frequency coupling behavior and the number of harmonics considered is by the 20th-order harmonics for each component. Additionally, the high-order components are also taken into account to investigate the coupling behavior in high-frequency region.

The flow of the harmonics vector is shown in Fig. 2, where the buck converter is used as an example to explain how the harmonics vectors are updated to the other components during calculation. The harmonics vectors of the other converters can also be transferred to their components in a similar way. The small letter in Table I (a)–(c) means the time-domain signal. The capital letters in Fig. 2 and Table I (4)–(6) stand for the harmonic coefficient components, which are derived from the Fourier series.

Each block has its input (U) and output (Y) harmonic vectors, as shown in Fig. 2. In the case of a buck converter model, the module can be divided into three blocks, namely, the "*L–R* circuit," the "*R–C* circuit," and the "switch circuit." The time-domain switching function is reorganized into a Toeplitz (Γ) [20] matrix to perform a convolution, as shown in Fig. 2 (SW). First, the dc input voltage harmonic vector (V_{in}) is convoluted with switching Toeplitz matrix (SW). The results can be the input vector (V_{I}) of the "*L–R* circuit." Another input vector (V_{out}) of the "*L–R* circuit" can be derived from the "*R–C* circuit." The result (I_{L}) of the "*L–R* circuit" is the input vector of the "*R–C* circuit," where the "*R–C* circuit" includes the load (*R*) information and this can be changed into the current/voltage source. The inductor current (I_{L}) vector can also be convoluted with the switching vector (SW) to calculate the input vector of the input current harmonic (I_{in}). Conclusively, all input, output, and state harmonics vectors are iteratively updated, as shown in Fig. 2. The harmonic vector flow of other topologies can also be adapted in a similar way.

By using each achieved model, the simulation of multiple dc–dc converters is possible. A similar approach using the generalized averaging (GAV) [3] is researched to reduce the simulation time as well as the complexity. However, the GAV normally adapts a harmonics having a large magnitude than other harmonics relatively. Hence, it is difficult to see the correct frequency interaction, which is caused by other frequencies. The importance of this characteristic is noticeable when the dc–dc converters are connected with an ac–dc converter interface such as wind turbine, photovoltaics, microturbine, and ac loads. However, the HSS model can investigate how the harmonics are related intuitively because of the modularity of the components as shown in Fig. 2 and Table I.

C. Controller Modeling

In this paper, the dc output is only considered as a target to control the dc–dc converter in order to take into account the controller interaction in the dc–dc converter model. However, in order to account for the dynamics caused by nonlinear switching, the controller should also be linearized as the case of the linearized topology model in Fig. 2.

The different procedures can be compared with the time-domain simulation. In the calculation procedure of the time-domain results, the product of two time-domain signals can be represented as shown

$$\mathrm{out}\,(t) = u\,(t) \cdot \mathrm{in}\,(t) \tag{7}$$

where in(t) and out(t) are the input and the output signals, respectively, and $u(t)$ is the time signals to change the formulation of the input. For instance, $u(t)$ can be a switching signal sw(t) or a nonlinear component like an inductor. Contrary to (7), the linearized harmonics vector can be considered in the HSS model to reflect the variation of the non-LTV components $u(t)$, as shown

$$\Delta\mathrm{OUT}\,(t) = U_{\mathrm{base}} \cdot \Delta\mathrm{IN}\,(t) + \Delta U\,(t) \cdot \mathrm{IN}_{\mathrm{base}} \tag{8}$$

where U_{base}, $\mathrm{IN}_{\mathrm{base}}$ are the harmonics vectors of the previous state and $\Delta\mathrm{IN}(t)$, $\Delta U(t)$ are the small variations of the harmonics vectors ($\mathrm{IN}(t)$, $U(t)$). The division of two time-domain signals can also be linearized into harmonics vector representation by means of the partial differentiation as shown in (7) and (8).

The block diagram of the generalized dc-voltage controller is shown in Fig. 3, where the signals with small letters are the

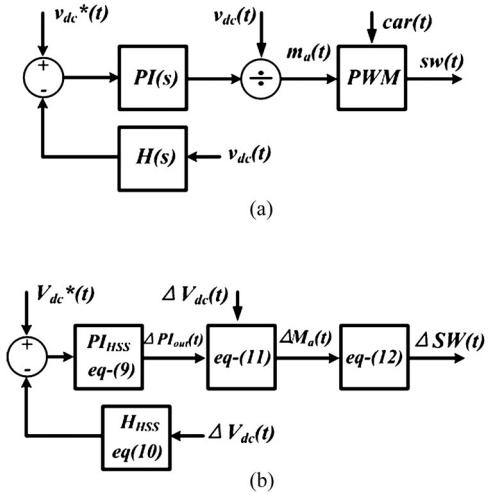

Fig. 3. Block diagram of a generalized controller for the dc–dc converter. (a) Nonlinear simulation model for the time-domain signals. (b) Linearized simulation model for the HSS model, where the harmonic vectors (capital) are used as the signals.

time-domain signals and the signals with capital letters mean the harmonics vectors, including both the 20th-order harmonics and high-frequency range ($0.5f_{\rm sw}\ldots, 2f_{\rm sw}, 3f_{\rm sw}\ldots$) in the vector. According to the procedure given in (7) and (8), the nonlinear time-domain model in Fig. 3(a) can be linearized into the HSS model as shown in Fig. 3(b). The detailed equations derived from the linearization procedure are shown in (9)–(12)

$$\mathrm{PI}_{\rm HSS}=\begin{bmatrix}\mathrm{PI}\left(s-jh\omega_0\right) & & & \\ & \ddots & & \\ & & \mathrm{PI}\left(s\right) & \\ & & & \ddots \\ & & & \mathrm{PI}\left(s+jh\omega_0\right)\end{bmatrix} \tag{9}$$

where $PI(s)=K_p+K_i/s$, K_p is the proportional gain, K_I is the integrator gain, and $\mathrm{PI}_{\rm HSS}$ is the HSS format of $\mathrm{PI}(s)$

$$H_{\rm HSS}=\begin{bmatrix}H\left(s-jh\omega_0\right) & & & \\ & \ddots & & \\ & & H\left(s\right) & \\ & & & \ddots \\ & & & H\left(s+jh\omega_0\right)\end{bmatrix} \tag{10}$$

where $H(s)=1/(s\cdot K_{\rm lpf}+1)$, with $K_{\rm lpf}$ being the low-pass filter bandwidth and $H_{\rm HSS}$ being the HSS format of $H(s)$

$$\Delta M_a\left(t\right)=-\frac{PI^b_{\rm out}}{\left(V^b_{\rm dc}\right)\Gamma\left(V^b_{\rm dc}\right)}\Delta V_{\rm dc}\left(t\right)+\frac{1}{V^b_{\rm dc}}PI_{\rm out}\left(t\right) \tag{11}$$

where $V^b_{\rm dc}$, $PI^b_{\rm out}$ are the previous state values and $\Delta V_{\rm dc}(t)$, $\Delta\mathrm{PI}_{\rm out}(t)$, and$\Delta M_a(t)$ are the updated states of the dc voltage, the output of PI controller, and the modulation index, respectively

$$\Delta\mathrm{SW}\left(t\right)=\Gamma\left(\mathrm{SW}_n-\mathrm{SW}_{n-1}\right)\Delta M_a\left(t\right) \tag{12}$$

where SW_n, SW_{n-1} are, respectively, the present status and the previous status of the PWM harmonics vector.

The updated harmonics vectors in Fig. 3(b) are continuously transferred to the state vector of the dc–dc converter to update the state. The same linearized dc-voltage controller is used in the three different topologies with various controller gains and references. Additionally, regarding the controller scheme, the different types can be modeled by using the HSS method. First, the low-pass filter used in this paper is to filter out the switching ripple of dc voltage because the PI controller used in the controller in Fig. 3 has a high gain at a dc frequency region. However, it can directly be sensed by using a voltage divider as well. Second, the reason why the output signal of the PI controller is divided by $v_{\rm dc}$ is to scale down the controller output before it is compared with the saw-tooth carrier signal. The sensed voltage or current signals in the controller are generally scaled up or down to adjust the magnitude of signals. The used controller scheme in this paper can be changed by various ways.

D. Low-Voltage DC-Cable Modeling

To consider the interaction caused by the connection of cable and converter, a low-voltage dc-cable is also modeled. Instead of using a simple inductance or resistance model, the PI-section model is taken into account according to the length of the cable. The derived result is shown in Table II, where the HSS modeling theory (1)–(3) is also used to include the harmonics in the model and $G_{\rm PI}$, $C_{\rm PI}$, $L_{\rm PI}$, and $R_{\rm PI}$ are, respectively, the conductance, the capacitance, the inductance, and the resistance of the PI-section cable model. In addition, the acronyms and subscripts used in (13) have also the same meaning as in (4)–(6). The achieved cable model can be combined with other converters and loads, as shown in Fig. 1 (Cable #1 to Cable #12). An ac-cable is considered in the dc-grid system to adapt practical data for simulations. The used cable data are as follows [25]:

1) current rating: 200 A;
2) cable type: three-conductor A1-PVC 185 mm^2;
3) resistance: 0.152 mΩ/m;
4) inductance: 0.237 μH/m;
5) capacitance: 2 pF/m (assumed);
6) cable length: 1000 m (Cable #1 to Cable #12).

The conductance is not taken into account in the parameters, and the capacitance is determined as the assumed values. However, the effect of the capacitance can be neglected because the dc system does not need to consider the reactive power driven by the parasitic capacitance of the cable.

III. HSS Simulation Results

To validate the modeling and analysis results of the dc power electronics system, MATLAB and PLECS are used for time and frequency domain simulations to illustrate the two different assessment methods. All the simulations have been performed using i7-4800MQ CPU (2.7 GHz). The presented dc–dc converter models in Section II are used to validate the dc power electronic systems.

TABLE II
CIRCUIT DIAGRAM AND HSS MODELING OF LOW-VOLTAGE DC CABLE: (A) CIRCUIT DIAGRAM OF CABLE MODEL (PI SECTION), WHERE Z IS THE ZERO MATRIX

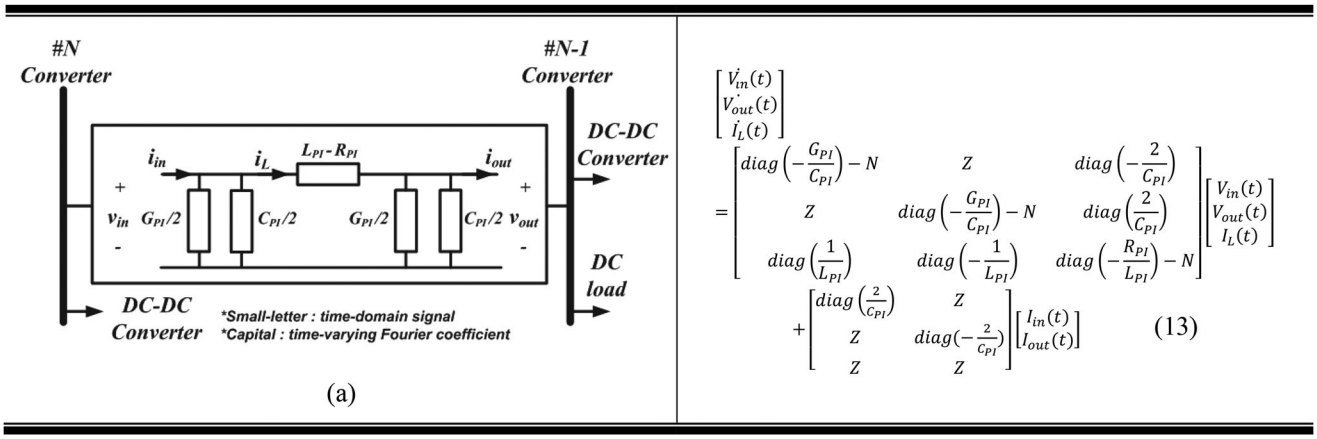

$$\begin{bmatrix} \dot{V}_{in}(t) \\ \dot{V}_{out}(t) \\ \dot{I}_L(t) \end{bmatrix} = \begin{bmatrix} diag\left(-\frac{G_{PI}}{C_{PI}}\right) - N & Z & diag\left(-\frac{2}{C_{PI}}\right) \\ Z & diag\left(-\frac{G_{PI}}{C_{PI}}\right) - N & diag\left(\frac{2}{C_{PI}}\right) \\ diag\left(\frac{1}{L_{PI}}\right) & diag\left(-\frac{1}{L_{PI}}\right) & diag\left(-\frac{R_{PI}}{L_{PI}}\right) - N \end{bmatrix} \begin{bmatrix} V_{in}(t) \\ V_{out}(t) \\ I_L(t) \end{bmatrix} + \begin{bmatrix} diag\left(\frac{2}{C_{PI}}\right) & Z \\ Z & diag\left(-\frac{2}{C_{PI}}\right) \\ Z & Z \end{bmatrix} \begin{bmatrix} I_{in}(t) \\ I_{out}(t) \end{bmatrix} \quad (13)$$

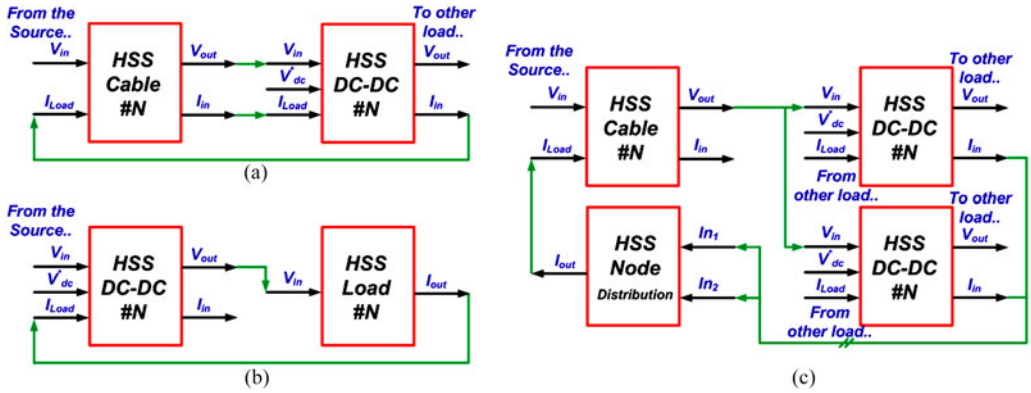

Fig. 4. Block diagram for the connection of each HSS module into a full simulation cases. (a) DC–DC converter connection with single cable, (b) dc–dc converter connection with single load, and (c) two parallel connected dc–dc converters connected with a single input cable.

A. Simulation Parameters

To show the switching ripple in the simulation, the switching frequency of each dc–dc converter is assumed to be 5 kHz. The bus #1 in Fig. 1 is assumed as 200 V_{dc}. Based on the dc voltage of the main bus (Bus #1), the dc voltage is boosted by using the dc–dc converters (#1 to #3). The buck converters (#4, #9) are considered to step down the voltage for the loads (#1, #3). The buck–boost converters (#5, #6) are deemed to control the dc voltage in order to manage a time-varying dc voltage (BESS, PV, fuel cell). Also, the boost converters (#7, #8) are taken into account to step up the voltage for the load and for a wind turbine, as shown in Fig. 1. For the simplicity of the simulation model, the outputs of PV, BESS, and wind turbine are assumed to have a constant dc voltage. The resistive loads are only considered for the simulations. However, the proposed simulation model can be extended to connect to the constant voltage loads, constant power loads, and other *RLC* loads.

B. HSS Module Connection

To connect the developed HSS module in the previous section, it is required to link both the input and output harmonics vectors into a final model. Three examples are shown in Fig. 4 to explain how the HSS module can be connected to each other, where the capital means the harmonics vector as given in (2).

The final input and output vectors of each dc–dc converter can be defined by the dc voltage reference (V_{dc}^{*}), the input voltage (V_{in}), and the output load current (I_{load}), in addition the output voltage (V_{out}) and the input current (I_{in}) are the output harmonics vectors. The cables and loads can also be similarly defined. The definition of input and selection of output channels can be adjusted according to the user's choice.

The cable and single converters can be connected, as shown in Fig. 4(a), where the output voltage of the cable can be linked to the input voltage of the dc–dc converters and the current input vector of dc–dc converters is connected to the output harmonics vector of the cable. The connection with the dc–dc converter and load can also be made, as shown in Fig. 4(b). However, in the case of parallel connection of converters or cables, a node distribution matrix ($\mathrm{Dist}_{\mathrm{node}}$) is required to divide or to combine the multicurrent/voltage signals, simultaneously, as shown in Fig. 4(c). The formulation to do this can be defined as follows:

$$\mathrm{Dist}_{\mathrm{node}} = [\mathrm{eye}(k)_1,\ \mathrm{eye}(k)_2,\ \ldots \mathrm{eye}(k)_n] \quad (14)$$

where the $\mathrm{eye}(\cdot)$ means the identity matrix and the size of the matrix are dependent on the number of harmonics (k). Addition-

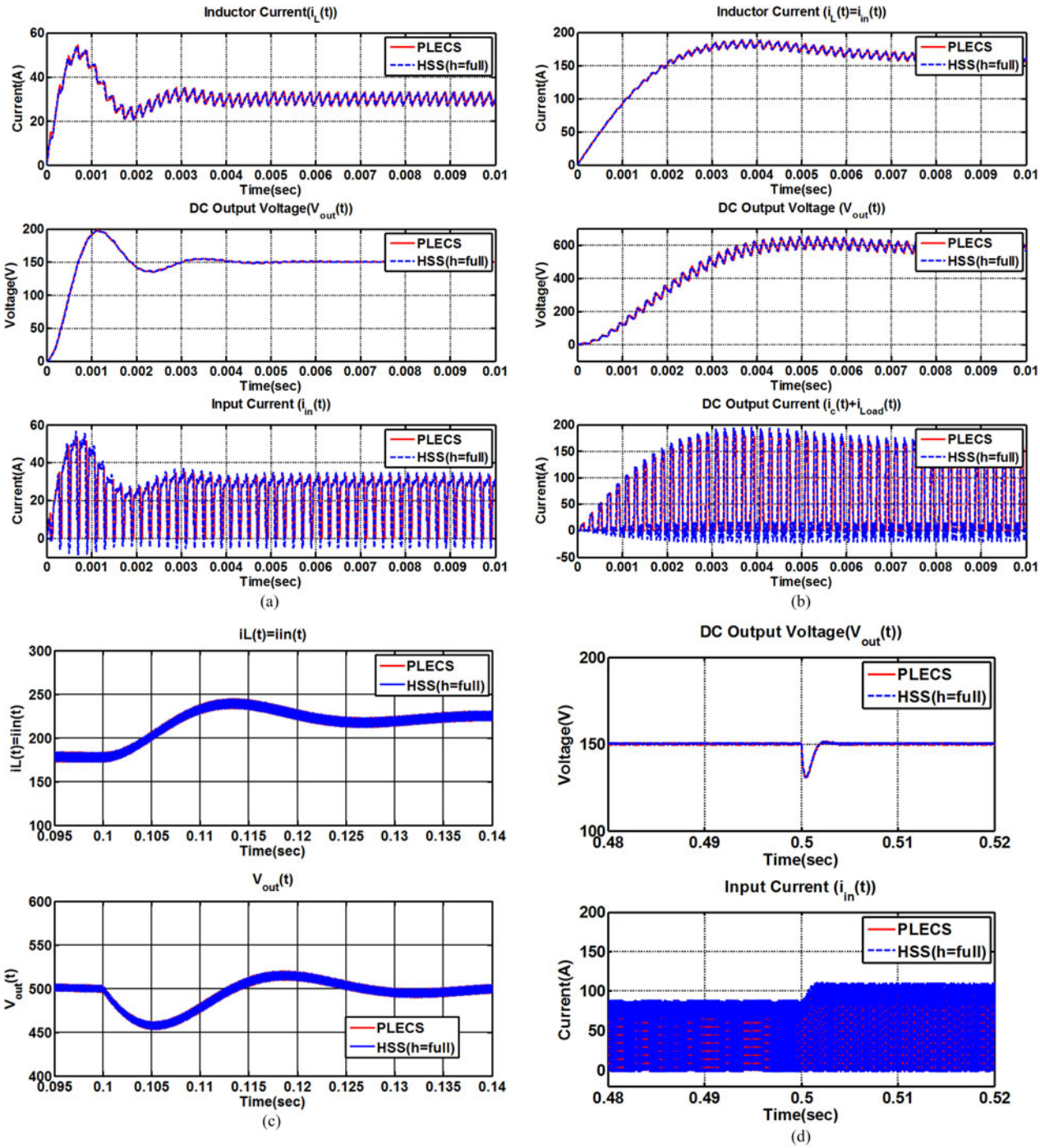

Fig. 5. Comparison of simulation results using the PLECS and HSS modeling (a) buck converter in Table I-(a), (b) boost converter in Table I-(b), (c) 20% dc-load (load converters) step of boost converter #5 at $t = 0.1$ ($i_{\mathrm{L}}(t) =$ inductor current, $v_{\mathrm{out}}\ (t) =$ dc output voltage), (d) 10% input-voltage reduction of buck converter #4 at $t = 0.5$ ($i_{\mathrm{in}}(t) =$ input current, $v_{\mathrm{out}}\ (t) =$ dc output voltage).

ally, "*n*" means the number of nodes to be added to one node. Through the connection module method described in Fig. 4, the other series and parallel connections can also be achieved.

C. Simulation (Steady State/Dynamic)

Based on the given parameters, the simulations and comparisons are derived, as shown in Fig. 5. The harmonic vector obtained from (1) can be converted into the time domain by rotating with the harmonic frequency. The summation of each harmonics into a time-domain signal is then shown in Fig 5. The results show that the HSS simulations are matched well with the nonlinear time-domain simulations (PLECS), as shown in Fig 5.

The simulation results are tested with two cases. First, a transient state from the starting point is tested to validate

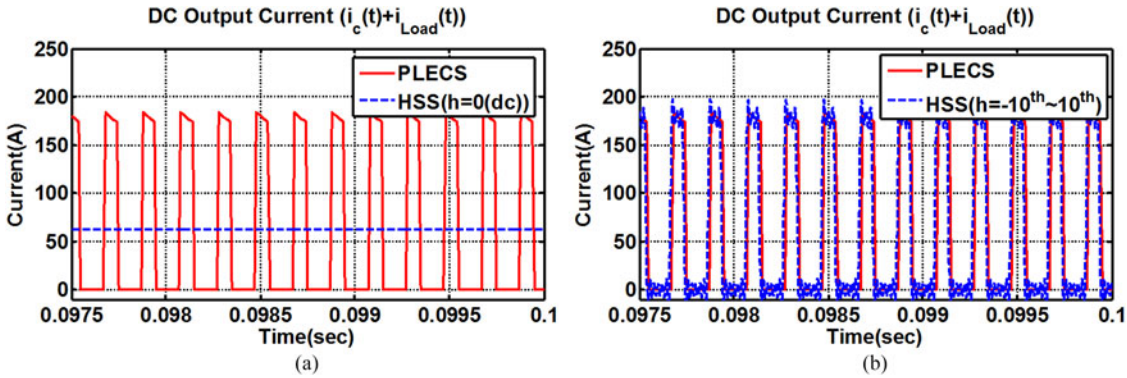

Fig. 6. Comparison of simulation precision according to the number of harmonics ($i_c(t)$ = capacitor current, $i_{\mathrm{Load}}(t)$ = output load current): (a) comparison of PLECS and HSS [$h = 0$(dc)] and (b) comparison of PLECS and HSS ($h = -10$th to 10th).

the calculation and convergence from the "zero" initial state. Second, the dynamic behavior from steady state is also simulated to test both the switching instant variation and the update of the previous state value. Besides that, the accuracy of the simulation result is also discussed with the comparison. The constant dc voltage (200 $\mathrm{V_{dc}}$) is stepped down to 150 $\mathrm{V_{dc}}$, as shown in Fig. 5(a). The main dc bus (Bus #1) is converted into 500 $\mathrm{V_{dc}}$ through a boost converter, as shown in Fig. 5(b). Using the buck–boost converter, 500 $\mathrm{V_{dc}}$ is also converted into 250 $\mathrm{V_{dc}}$. The results indicate well the transient state from the starting point and the convergence of the steady state.

Furthermore, the dynamic response of the buck and boost converters during the steady state, which happens when connecting to the other load converters (at $t = 0.1$), shows the same results with the nonlinear time-domain simulation, as shown in Fig. 5(c). According to the increased load, the output voltage converges to steady state and the load current is increased simultaneously. The output dc voltage is also tracking the reference voltage again, as shown in Fig. 5(d), even if the dc input voltage is changed. The input current is thus increased to keep the same output power during the operation.

Compared to the nonlinear time-domain simulation and the other modeling methods, the accuracy of the simulation depends on the number of harmonics and the precision of the Fourier series. The compared results are shown in Fig. 6(a) and (b); the results show that the precision can be increased by increasing the number of harmonics. However, the calculation time will be increased due to the size of the matrix.

In a simulation of a single converter, the nonlinear time-domain simulation is faster than the HSS model. However, the HSS model has similar performance. For instance, the 1st to 20th harmonics can be considered to analyze low-frequency coupling caused by ac–dc and dc–dc converters. Besides, switching harmonics and its multiple harmonics can also be a part to emulate the switching ripple. Otherwise, the switching frequency of the dc–dc converter can only be considered for the analysis of dc–dc converters. Furthermore, the HSS model has more advantages as the number of circuits increase. The calculation time of the long-term HSS simulation is also shorter than the nonlinear time-domain simulation. The comparison of two methods is shown in Table III.

TABLE III
SIMULATION TIME COMPARISON

Simulation Condition (Module/Simulation Time)	PLECS	HSS
1 converter/1 s	6 s.	7 s.
9 converters, 3 load/1 s	50 min	4 min

Controllers are all included in the module.

D. Detailed Dynamic Behavior of Harmonic Vectors

One particular case is depicted later where the relationship between the small variation of dc voltage (ΔV_{out}) and the responses of switching instant variations ($\Delta\mathrm{SW}$) is explained.

First, the nonlinear behavior of (7) is explained by means of Fig. 7(a) and (b). The saw-tooth carrier signal (v_{car}) is compared with the controlled reference signal (v_{ref}) and the result is the PWM signal, as shown in Fig. 7(b). The variation of the reference signal at a certain time may also bring the variation of switching signal $\Delta\mathrm{sw}(t)$, as shown in Fig. 7(b). This difference can be calculated and reflected in the nonlinear time-domain simulation by finding a convergence point with iteration. However, it may take time for increasing the number of simulation target because it needs to find various convergence points. In the case of HSS method, (8) can be used to emulate the behavior of (7) where "base" means the previous state values. Contrary to Fig. 7(b), the variation of switching instant in HSS method is represented by varying multiple harmonics, as shown in Fig. 7(c). It is noted that all harmonics of $\Delta\mathrm{sw}(t)$ are represented by $\Delta\mathrm{SW}_{-h\ldots h}(t)$. As a result, the variation of the dc voltage, inductor current, and control output can be reflected by using (8), which is composed by varying multiple harmonics. This approach does not require a calculation of convergence point at a zero crossing point. Furthermore, the frequency coupling behaviors driven by switching are included at steady state as well as at dynamic state. The simulation results of a buck converter are depicted in Fig. 7(d)–(f), where the dc voltage reference is changed from 100 to 120 V at 1 s. The linearized varying switching harmonics are involved with the previous harmonic state value of dc voltage and inductor current to reflect the dynamics driven by nonlinear switching according to (8). All

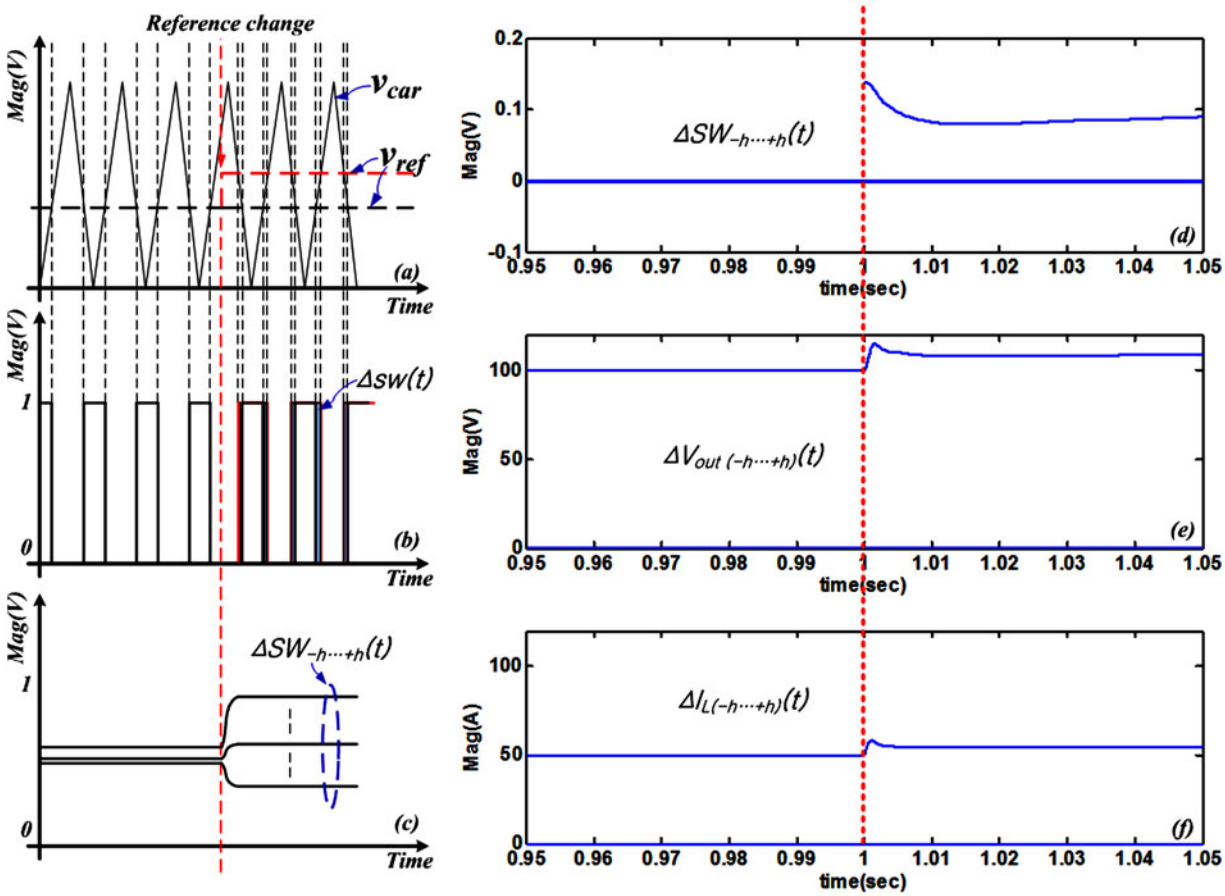

Fig. 7. Detailed description of the small-variation (Δ) behaviors: (a) time-domain representation of carrier signal ($v_{\rm car}$) and reference signal ($v_{\rm ref}$), where the changed reference is in red color, (b) time-domain representation of PWM signal and small variation of switching signal $\Delta {\rm sw}(t)$, (c) HSS direct simulation of switching instant variation, where all signals are varying harmonics ($-h, \ldots, h$), (d) direct HSS simulation result of switching instant variation $\Delta {\rm SW}_{-h\ldots+h}(t)$, (e) direct HSS simulation result of dc-voltage variation $\Delta V_{{\rm out}(-h\ldots+h)}(t)$, and (f) direct HSS simulation result of inductor current variation $\Delta I_{L(-h\ldots+h)}(t)$.

varying harmonics are shown in Fig. 7(d)–(f), where it is possible to investigate how harmonics are changed and converted. Though the variation of harmonics except the dc component is small in Fig. 7(d)–(f), those are containing the possibility to be involved in a frequency transfer from input or other nodes. All switching behaviors used in this paper are using (7) and (8) and are operated as shown in Fig. 7.

E. Discussion About Frequency Coupling

The HSS modeling and simulation results are verified by means of comparison with nonlinear time-domain simulation in the earlier section. It is worth noting that the HSS shows exactly the same harmonics and ripple shown in the time-domain simulation. It is possible due to the consideration of switching instant behavior and its continuous update, which cannot be included in the conventional modeling method, for instance, GAV and SSAV. The frequency coupling causes the frequency transfer from one side to the other side, another frequency generation and mitigation through switching. Hence, this section explains the details and theory how this frequency coupling effect can be shown in HSS model by means of an example.

The buck converter is considered as an example to validate the availability of frequency coupling analysis in HSS model. The assumed case is low-frequency coupling when the ac–dc converter is connected to the input or output dc voltage of the dc–dc converter, which can be a common case as dc-network application is increasing. The fundamental frequency (f_s) of ac–dc converter generates $2f_s,\ 4f_s, \ldots,$ in single-phase ac–dc converter applications and $6f_s,\ 12f_s, \ldots,$ in three-phase applications due to the frequency coupling through the modulation. Even though various ways have been researched to mitigate these harmonics, there are pros and cons. For instance, the proportional resonant controller can compensate harmonics. However, it also generates another harmonics or adjusts the stable region of the system [26], [27]. Hence, it is needed to investigate the nature of the low-frequency coupling between the ac–dc converter and the dc–dc converter.

Passive elements and switching frequency used in the buck converter (#4) is used for simulation. The low-frequency oscillation in the dc input voltage is defined as 100 Hz (10%) under the assumption, where the single-phase ac–dc converter is connected to the input of the dc–dc converter. The modulation procedure between the input and output filters can be simply represented as given in (15), where $v_{\rm dc_{in}}(t)$ is the input voltage, $d(t)$ is the modulation ratio, ω_s is the low-frequency component of the input voltage, ω_d is the low-frequency component in modulation, $v_{\rm out}(t)$ is output voltage by means of modulation,

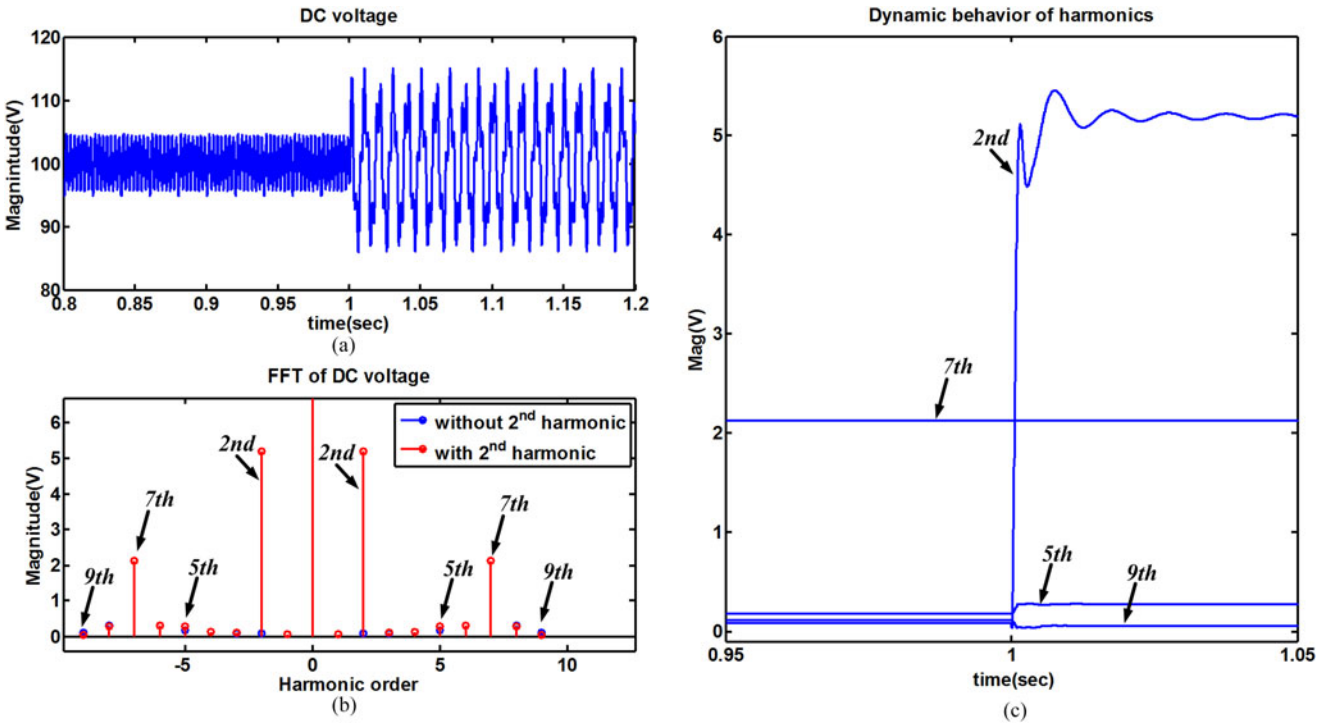

Fig. 8. Buck converter simulation result for frequency coupling effect: (a) HSS simulation result of dc output voltage, (b) FFT result of dc output voltage, and (c) dynamic behavior of harmonics in dc voltage.

another high-frequency components are aggravated as "...," and β, α are the small ratios of the low-frequency component to represent the varying modulation index

$$v_{\text{out}}(t) = [d(t)\cdot(1+\alpha\cdot\cos(\omega_d t)+\cdots)] \cdot[v_{\text{dc}_{\text{in}}}(t)\cdot(1+\beta\cdot\cos(\omega_s t)+\cdots)]. \quad (15)$$

It is worth noting that (15) shows the ordinary duty ratio equation between the input and the output, if α, β are equal to "0." Otherwise, α, β can be assigned according to the operation, where α can be defined based on the load condition and β can also be decided depending on the topology connected to the dc input. Additionally, the other possible frequency can be inserted to the both the input and the duty oscillation. Coupled frequency components shown in the output side can be simply represented as given in (16)–(18), where $v_{\text{out}_{\text{dc}}}(t)$ is the dc term of (15), $v_{\text{out}_{\text{low}}}(t)$ is the low-frequency nature from both input and modulation, and $v_{\text{out}_{\text{cross}}}(t)$ is the coupled frequency driven by the multiplication of two frequencies

$$v_{\text{out}_{dc}}(t) = v_{\text{dc}_{\text{in}}}(t)\cdot d(t) \quad (16)$$

$$v_{\text{out}_{\text{low}}}(t) = v_{\text{dc}_{\text{in}}}(t)\cdot d(t)\cdot\alpha\cdot\cos(\omega_d t) + v_{\text{dc}_{\text{in}}}(t)\cdot d(t)\cdot\beta\cdot\cos(\omega_s t) \quad (17)$$

$$v_{\text{out}_{\text{cross}}}(t) = (v_{\text{dc}_{\text{in}}}(t)\cdot d(t)\cdot\alpha\cdot\beta)/2\cdot[\cos((\omega_d+\omega_s)t) + \cos((\omega_d-\omega_s)t)]. \quad (18)$$

The frequency coupling driven by other added frequency can also be explained in a similar way. However, note that all behaviors in (16)–(18) are non-LTV. Hence, it is difficult to emulate in a conventional way because of averaging and the nature of LTI system (SISO). According to the described modeling and simulation procedure, the HSS simulation result of the buck converter is shown in Fig. 8 that 100 Hz (second order) harmonics are shown with a switching ripple and dc component, where this frequency is transferred from the input frequency. The switching function includes the seventh-order harmonic before the second-order harmonic is perturbed into the dc–dc converter. The result in Fig. 8 shows that the injected second-order harmonic at 1 s affects to the other side low-order harmonics (fifth and ninth), where the fifth harmonic is increased and the ninth harmonic is decreased according to (15)–(18). The dynamic behavior of each harmonic shows different transient responses, which means all harmonics have different frequency responses. It is noted that the transformation of Fig. 8(c) by using (2) is exactly the same as Fig. 8(a). Hence, it is noticeable that the nonlinear behavior of (16)–(18) correctly reflects the final simulation result by means of HSS method since the LTP model can show multiple frequency output characteristic from multiple sinusoidal inputs and show how the frequency is coupled, attenuated, and canceled each other.

F. Short Discussion About the Asynchronous Behavior

The fundamental structure of HSS method is based on the theory of the LTP system where it is assumed that all signals and parameters vary periodically. Hence, if the test object does not have a periodic status, the HSS method is difficult to be used in the analysis, and this could be a limitation of this method. However, it has been researched in [20]–[22], [28], and [29]

that almost all power electronic systems include the periodic behavior and that the frequency coupling behavior are mainly appeared by means of the periodic interaction. Additionally, the interharmonics that can normally be investigated in the ac–dc application have been analyzed with the HSS (HD) method [30], [31] by selecting a base frequency as 0.1 Hz, 0.5 Hz, etc. Though the matrix size could be huge in this case, several methods, including a sparse matrix, have been studied to reduce the matrix size, which is quite related with the computation time. However, the simulation of this small range frequency coupling would take more time in the nonlinear time-domain simulation because it needs to reduce a time step more and it consequently brings a huge simulation time for a large system. Furthermore, even if the system has an asynchronous feature in the operation, as long as the system has the periodic properties, the system has the possibility to be analyzed by the HSS method. The diode and thyristor applications, which have the characteristic of parameter-dependent switching have also researched in [20] and [29]. The asynchronous switching behavior is modeled by the HSS method, and the result shows an accurate simulation result compared to the nonlinear time-domain simulation.

IV. Conclusion

This paper presents the modeling and simulation of dc power electronic systems by using an HSS modeling approach. Each component, as well as the dc–dc converters, is modularized to connect it with other models. The selected converters are analyzed and validated by means of the proposed method. To verify the validity of the HSS model, the HSS simulation results are compared with the nonlinear time-domain simulation. Also, the frequency coupling between the source of the power converters and the output of power converters is also analyzed. The overall results derived from the HSS model show the same performance, which means the transfer function derived from HSS model has more accurate characteristic than the conventional modeling method, e.g., SSAV or GAV. Besides, the whole dc–dc converters are simulated by using HSS method for the large-scale network. The result shows that the HSS can provide faster simulation time with the same result with nonlinear time-domain simulation. Furthermore, the model proposed in this paper can include various harmonics, where it can be used for the analysis of harmonic interactions, the design of the controller or the stability assessment, which cannot be found in the LTI model.

References

[1] J. B. Kwon, X. Wang, C. L. Bak, and F. Blaabjerg, "Modeling and simulation of DC power electronics systems using harmonic state space (HSS) method," in *Proc. IEEE 16th Workshop Control Model. Power Electron.*, 2015, pp. 1–8.

[2] K. J. Karimi, A. Booker, and A. Mong, "Modeling, simulation, and verification of large DC power electronics systems," in *Proc. 27th Annu. IEEE Power Electron. Spec. Conf. Record*, 1996, vol. 2, pp. 1731–1737.

[3] A. Emadi, "Modeling and analysis of multiconverter DC power electronic systems using the generalized state-space averaging method," *IEEE Trans. Ind. Electron.*, vol. 51, no. 3, pp. 661–668, Jun. 2004.

[4] X. Wang, F. Blaabjerg, and W. Wu, "Modeling and analysis of harmonic stability in an AC power-electronics-based power system," *IEEE Trans. Power Electron.*, vol. 29, no. 12, pp. 6421–6432, Dec. 2014.

[5] R. D. Middlebrook, "Small-signal modeling of pulse-width modulated switched-mode power converters," *Proc. IEEE*, vol. 76, no. 4, pp. 343–354, Apr. 1988.

[6] K. K. Tse, H. S.-H. Chung, S. Y. R. Hui, and H. C. So, "A comparative study of carrier-frequency modulation techniques for conducted EMI suppression in PWM converters," *IEEE Trans. Ind. Electron.*, vol. 49, no. 3, pp. 618–627, Jun. 2002.

[7] J. Balcells, A. Santolaria, A. Orlandi, D. Gonzalez, and J. Gago, "EMI reduction in switched power converters using frequency Modulation techniques," *IEEE Trans. Electromagn. Compat.*, vol. 47, no. 3, pp. 569–576, Aug. 2005.

[8] W. Yan, W. Li, and R. Liu, "A noise-shaped buck DC #x2013;DC converter with improved light-load efficiency and fast transient response," *IEEE Trans. Power Electron.*, vol. 26, no. 12, pp. 3908–3924, Dec. 2011.

[9] D. J. Perreault and G. C. Verghese, "Time-varying effects and averaging issues in models for current-mode control," *IEEE Trans. Power Electron.*, vol. 12, no. 3, pp. 453–461, May 1997.

[10] S. R. Sanders, J. M. Noworolski, X. Z. Liu, and G. C. Verghese, "Generalized averaging method for power conversion circuits," *IEEE Trans. Power Electron.*, vol. 6, no. 2, pp. 251–259, Apr. 1991.

[11] F. Yahyaie and P. W. Lehn, "On dynamic evaluation of harmonics using generalized averaging techniques," *IEEE Trans. Power Syst.*, vol. 30, no. 5, pp. 2216–2224, Sep. 2015.

[12] J. Mahdavi, A. Emaadi, M. D. Bellar, and M. Ehsani, "Analysis of power electronic converters using the generalized state-space averaging approach," *IEEE Trans. Circuits Syst. Fundam. Theory Appl.*, vol. 44, no. 8, pp. 767–770, Aug. 1997.

[13] V. Vorperian, "A ripple theorem for PWM DC-to-DC converters operating in continuous conduction mode," in *Proc. IEEE 35th Annu. Power Electron. Spec. Conf.*, 2004, vol. 1, pp. 28–35.

[14] P. Patra, A. Patra, and N. Misra, "A single-inductor multiple-output switcher with simultaneous buck, boost, and inverted outputs," *IEEE Trans. Power Electron.*, vol. 27, no. 4, pp. 1936–1951, Apr. 2012.

[15] X. Yue, F. Wang, S. Yang, F. Zhuo, and Y. Pei, "Modeling for input impedance of buck converters and its application analysis," in *Proc. IEEE Energy Convers. Congr. Expo.*, 2015, pp. 2400–2406.

[16] X. Yue, Y. Zhu, S. Yang, Y. Chen, F. Zhuo, and Y. Pei, "A modulation and sampling based modeling method for the nonlinearities of power converters and its application analysis," in *Proc. 17th Eur. Conf. Power Electron. Appl. ECCE Europe*, 2015, pp. 1–10.

[17] J. Arrillaga and N. R. Watson, "The harmonic domain revisited," in *Proc. 13th Int. Conf. Harmonics, Quality, Power*, 2008, pp. 1–9.

[18] B. Vyakaranam, M. Madrigal, F. E. Villaseca, and R. Rarick, "Dynamic harmonic evolution in FACTS via the extended harmonic domain method," in *Proc. Power Energy Conf. Illinois*, 2010, pp. 29–38.

[19] E. Mollerstedt and B. Bernhardsson, "Out of control because of harmonics-an analysis of the harmonic response of an inverter locomotive," *IEEE Control Syst.*, vol. 20, no. 4, pp. 70–81, Aug. 2000.

[20] J. R. C. Orillaza and A. R. Wood, "Harmonic state-space model of a controlled TCR," *IEEE Trans. Power Del.*, vol. 28, no. 1, pp. 197–205, Jan. 2013.

[21] M. S.-P. Hwang and A. R. Wood, "A new modelling framework for power supply networks with converter based loads and generators—The harmonic state-space," in *Proc. IEEE Int. Conf. Power Syst. Technol.*, 2012, pp. 1–6.

[22] M. S. Hwang and A. R. Wood, "Harmonic state-space modelling of an HVdc converter," in *Proc. IEEE 15th Int. Conf. Harmonics Quality Power*, 2012, pp. 573–580.

[23] N. M. Wereley and S. R. Hall, "Linear time periodic systems: Transfer function, poles, transmission zeroes and directional properties," in *Proc. Amer. Control Conf.*, 1991, pp. 1179–1184.

[24] J. Kwon, X. Wang, C. L. Bak, and F. Blaabjerg, "Harmonic interaction analysis in grid connected converter using harmonic state space (HSS) modeling," in *Proc. IEEE Appl. Power Electron. Conf. Expo.*, 2015, pp. 1779–1786.

[25] S. Anand and B. G. Fernandes, "Reduced-order model and stability analysis of low-voltage DC microgrid," *IEEE Trans. Ind. Electron.*, vol. 60, no. 11, pp. 5040–5049, Nov. 2013.

[26] A. G. Yepes, F. D. Freijedo, O. Lopez, and J. Doval-Gandoy, "Analysis and design of resonant current controllers for voltage-source converters by means of nyquist diagrams and sensitivity function," *IEEE Trans. Ind. Electron.*, vol. 58, no. 11, pp. 5231–5250, Nov. 2011.

[27] J. Kwon, X. Wang, and F. Blaabjerg, "Impedance based analysis and design of harmonic resonant controller for a wide range of grid impedance," in *Proc. IEEE 5th Int. Symp. Power Electron. Distrib. Generation Syst.*, 2014, pp. 1–8.

[28] J. J. Rico, E. Acha, and T. J. E. Miller, "Harmonic domain modelling of three phase thyristor-controlled reactors by means of switching vectors and discrete convolutions," *IEEE Trans. Power Del.*, vol. 11, no. 3, pp. 1678–1684, Jul. 1996.
[29] E. Mollerstedt and B. Bernhardsson, "A harmonic transfer function model for a diode converter train," in *Proc. IEEE Power Eng. Soc. Winter Meeting*, 2000, vol. 2, pp. 957–962.
[30] G. N. Bathurst, N. R. Watson, and J. Arrillaga, "Adaptive frequency-selection method for a Newton solution of harmonics and interharmonics," *Gener. Transm. Distrib. IEE Proc.*, vol. 147, no. 2, pp. 126–130, Mar. 2000.
[31] A. Ramirez, "The modified harmonic domain: Interharmonics," *IEEE Trans. Power Del.*, vol. 26, no. 1, pp. 235–241, Jan. 2011.

JunBum Kwon (S'14) was born in Seoul, Korea, in 1982. He received the B.S and M.S degrees from the Department of Control and Instrumentation Engineering, Seoul National University of Science and Technology, Seoul, in 2007 and 2010, respectively. He is currently working toward the Ph.D. degree with the Department of Energy Technology, Aalborg University, Aalborg, Denmark.

He was a Research Engineer with the HVDC Rsearch and Development Center, LS Industrial Systems, Anayang, Korea, from 2010 to 2013. His current research interests include three-phase grid-connected inverter for renewable energy, harmonic analysis with modeling, insulation coordination design, and thyristor valve design for HVDC.

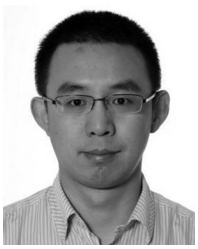

Xiongfei Wang (S'10−M'13) received the B.S. degree from Yanshan University, Qinhuangdao, China, in 2006, the M.S. degree from Harbin Institute of Technology, Harbin, China, in 2008, both in electrical engineering, and the Ph.D. degree from Aalborg University, Aalborg, Denmark, in 2013.

Since 2009, he has been with the Aalborg University, Aalborg, Denmark, where he is currently an Assistant Professor in the Department of Energy Technology. His current research interests include modeling and control of grid-connected converters, harmonics analysis and control, passive and active filters, and stability of power-electronic-based power systems.

Dr. Wang received an IEEE Power Electronics Transactions Prize Paper award in 2014. He is the Associate Editor of the IEEE TRANSACTIONS ON INDUSTRY APPLICATIONS and the Guest Associate Editor of the IEEE JOURNAL OF EMERGING AND SELECTED TOPICS IN POWER ELECTRONICS Special Issue on Harmonic Stability and Mitigation in Power Electronics Based Power Systems and Special Issue on Distributed Generation.

Frede Blaabjerg (S'86–M'88–SM'97–F'03) received the Ph.D. degree from Aalborg University, Aalborg, Denmark, in 1992.

He was with ABB-Scandia, Randers, Denmark, from 1987 to 1988. He became an Assistant Professor in 1992, an Associate Professor in 1996, and a Full Professor of Power Electronics and Drives in 1998 at Aalborg University. His current research interests include power electronics and its applications such as in wind turbines, PV systems, reliability, harmonics, and adjustable speed drives.

Dr. Blaabjerg has received 17 IEEE Prize Paper Awards, the IEEE PELS Distinguished Service Award in 2009, the EPE-PEMC Council Award in 2010, the IEEE William E. Newell Power Electronics Award 2014 and the Villum Kann Rasmussen Research Award 2014. He was an Editor-in-Chief of the IEEE TRANSACTIONS ON POWER ELECTRONICS from 2006 to 2012. He is nominated in 2014 and 2015 by Thomson Reuters to be between the most 250 cited researchers in engineering in the world.

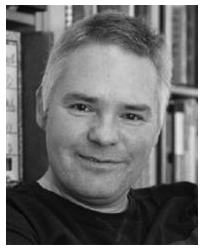

Claus Leth Bak (SM'99) was born in Århus, Denmark, on April 13th, 1965. He received the B.Sc. degree (with honors) in electrical power engineering, and the M.Sc. degree in electrical power engineering, in 1992 and 1994, respectively, and the Ph.D. degree, in 2015, with the thesis "EHV/HV underground cables in the transmission system." from the Department of Energy Technology (ET), Aalborg University (AAU), Aalborg, Denmark.

He was a Professional Engineer with the Electric Power Transmission and Substations with specializations within the area of Power System Protection at the NV Net Transmission Company. In 1999, he was an Assistant Professor at ET-AAU, where he is currently a Full Professor. He is the Head of the Energy Technology Ph.D. program (+ 100 Ph.D.s) and the Head of the Section of Electric Power Systems and High Voltage in AAU. He has supervised/cosupervised +30 PhDs and +50 MSc theses. His current research interests include Corona phenomena on overhead lines, power system modeling and transient simulations, underground cable transmission, power system harmonics, power system protection, and HVDC-VSC offshore transmission networks. He is the author or coauthor of app. 185 publications.

Dr. Bak is a Member of Cigré JWG C4-B4.38, Cigré SC C4 Study Committee Member, and Danish Cigré National Committee. He received the DPSP 2014 best paper award.